

**Precessional dynamics of elemental moments in a ferromagnetic alloy**

W. E. Bailey and L. Cheng

*Materials Science Program, Department of Applied Physics, Columbia University, New York, New York 10027, USA\**

D. J. Keavney

*Advanced Photon Source, Argonne National Laboratory, Argonne, Illinois 60439, USA*

C.-C. Kao, E. Vescovo, and D. A. Arena

*National Synchrotron Light Source, Brookhaven National Laboratory, Upton, New York 11973, USA*

(Received 17 June 2004; published 5 November 2004)

We demonstrate an element-specific measurement of magnetization precession in a metallic ferromagnetic alloy, separating Ni and Fe moment motion in  $\text{Ni}_{81}\text{Fe}_{19}$ . Pump-probe x-ray magnetic circular dichroism, synchronized with short magnetic field pulses, is used to measure free magnetization oscillations up to 2.6 GHz with elemental specificity and a rotational resolution of  $<2^\circ$ . Magnetic moments residing on Ni sites and Fe sites in a  $\text{Ni}_{81}\text{Fe}_{19}$  (50 nm) thin film are found to precess together at all frequencies, coupled in phase within instrumental resolution of 90 ps.

DOI: 10.1103/PhysRevB.70.172403

PACS number(s): 75.25.+z, 76.50.+g, 78.20.Ls, 78.47.+p

**I. INTRODUCTION**

The precession of magnetic moments in an applied magnetic field is relevant for many classes of materials studies. Precession is usually observed through microwave absorption, as in electron spin resonance (ESR), nuclear magnetic resonance (NMR), or ferromagnetic resonance (FMR), combining the response from all species present. In complex materials and heterostructures, time-domain optical techniques have proven useful to separate precessional dynamics at different atomic sites through the photon energy dependence of the response. Site-specific measurement of ESR<sup>1</sup> and NMR<sup>2</sup> precession has been achieved in semiconductors using visible optical pump-probe techniques. FMR precession of ferromagnetic alloys and heterostructures is technologically important since it determines data rates (switching speeds) of spin electronics devices.

The magnetic moments on *A* and *B* sites in a random ferromagnetic alloy  $A_{1-x}B_x$  are usually believed to be parallel and collinear, due to strong exchange forces, either in static equilibrium or precessional motion. However, noncollinear static moments are predicted as the ground state in random  $\text{Ni}_{1-x}\text{Fe}_x$  alloy systems, particularly near  $x=0.35$ .<sup>3</sup> The random site disorder plays a strong role in the reduction of collinearity, evidenced in the 30% reduction of exchange stiffness for  $x=0.75(\text{Ni}_3\text{Fe})$  upon an order-disorder transformation.<sup>4</sup> In  $\text{Ni}_{81}\text{Fe}_{19}$  (permalloy), total energy calculations predict a  $1^\circ-2^\circ$  average angle of moment noncollinearity at  $T=0$ .<sup>5</sup>

The magnetization dynamics of  $\text{Ni}_{81}\text{Fe}_{19}$  have been studied more intensively than those of any other alloy. Given the noncollinear ground-state alignment predicted for  $\text{Ni}_{81}\text{Fe}_{19}$ , it is natural to ask whether a small net misalignment of Ni and Fe moments may also exist in a low-energy configuration accessible at short times and finite temperatures. The different moments in the alloy ( $2.5$  vs  $1.6\mu_B/\text{atom}$ )<sup>6</sup> and different effective gyromagnetic ratios  $g_{\text{eff}}$  in elemental crystals

( $2.20$  vs  $2.11$ )<sup>7</sup> of Ni and Fe suggest different natural angular velocities for the motion of elemental moments. An element-specific measurement of magnetization precession can provide a direct test for the presence of a phase lag between  $\mathbf{M}_{\text{Ni}}$  and  $\mathbf{M}_{\text{Fe}}$  in coupled motion.

An element-specific measurement of ferromagnetic resonance (FMR) precession has not been available previously. An x-ray optical technique, x-ray magnetic circular dichroism (XMCD), is a well-established, quantitative, element-specific measurement of magnetic moment;<sup>8</sup> however, its previously demonstrated time-domain extension shows resolution of  $\sim 2$  ns. This has been sufficient to characterize  $180^\circ$  reversal dynamics in buried magnetic layers,<sup>9</sup> but is insufficient to characterize FMR precession at frequencies of  $f_p \geq 1$  GHz.

We present direct experimental separation of Ni and Fe magnetic moment precession in ferromagnetic  $\text{Ni}_{81}\text{Fe}_{19}$  (50 nm) through pump-probe XMCD. Improved time resolution ( $\sim 90$  ps FWHM) has been achieved in part through the use of a fast fall-time square wave magnetic field pulse delivered through a coplanar wave guide (CPW).<sup>10</sup> We verify coupled precession of elemental moments within instrumental resolution.

**II. EXPERIMENT**

Time-resolved XMCD (TR-XMCD) measurements were carried out at Beamline 4-ID-C of the Advanced Photon Source in Argonne, IL. The circular dichroism signal was obtained in reflectivity at near grazing incidence (see Fig. 1), using photon helicity  $\sigma$  switching ( $\sigma \parallel \hat{y}$ ) at the elliptical undulator for fixed applied field  $\mathbf{H}$ . Reflected intensity was read at a soft x-ray photodiode and normalized to an incident intensity at a reference grid. The measurement technique is photon-in/photon out and should therefore minimize artifacts from time-varying stray magnetic fields.

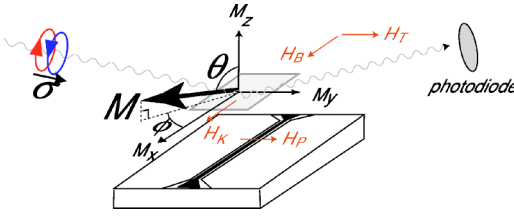


FIG. 1. (Color online) TR-XMCD measurement configuration. Circularly polarized photons are reflected at grazing incidence into a photodiode (right-hand side). XMCD is measured by switching photon helicity  $\sigma$ . Relative alignment of applied fields  $H_p$  (pulse),  $H_B$  (longitudinal bias),  $H_K$  (anisotropy), and  $H_T$  (transverse bias) is shown.

Time resolution was achieved through a pump-probe technique. Fast fall-time magnetic field pulses (pump) were synchronized with variable delay to x-ray photon bunches from the APS storage ring (probe). The repetition frequencies of photon bunches and magnetic field pulses were both 88.0 MHz (11.37 ns period); therefore, source or detector gating was not required.

The magnetic field delivery configuration is similar to that used in a pulsed inductive microwave permeameter (PIMM).<sup>10,11</sup> Fast fall-time current pulses ( $\sim 150$  ps) were delivered from a commercial pulse generator and through a CPW located under the magnetic thin film, providing pulsed transverse fields  $< 10$  Oe in amplitude. Pulses terminated into a 20 GHz sampling oscilloscope with 27 dB attenuation for pulse wave form characterization or directly into a 50  $\Omega$  load during TR-XMCD measurement. The CPW center conductor was aligned along  $\hat{x}$ , generating pulse fields  $\mathbf{H}_p = H_p \hat{y}$ . Orthogonal Helmholtz coils apply longitudinal bias  $\mathbf{H}_B = H_B \hat{x}$  or transverse magnetic field bias  $\mathbf{H}_T = H_T \hat{y}$ .

Experimental system time resolution can be estimated by using the finite photon bunch length  $\sigma_{ph}$ , and the timing jitter in the current pulse delivery electronics  $\sigma_{ij}$ . Separate streak camera measurements provide RMS bunch length  $\sigma_{ph} = 25$  ps (Ref. 12) and sampling oscilloscope measurements provide RMS timing jitter  $\sigma_{ij} = 30$  ps. Adding these contributions in quadrature yields a net timing resolution of  $\sqrt{\sigma_{ph}^2 + \sigma_{ij}^2} = 39$  ps RMS or 90 ps FWHM.

The  $\text{Ni}_{81}\text{Fe}_{19}$  (50 nm)/Ta (2 nm) thin film was deposited on the CPW using ion beam sputtering at a base pressure of  $5 \times 10^{-8}$  Torr. Magnetic anisotropy was induced using a static magnetic field applied along the center conductor, creating an effective uniaxial anisotropy field  $\mathbf{H}_K \parallel \hat{x}$ . The sample normal points along  $\hat{z}$ ; the plane of incidence of the

beam is  $yz$ , oriented roughly  $5^\circ$  off  $y$ . During TR-XMCD, magnetization was longitudinally biased,  $0 < H_B < 100$  Oe along the easy anisotropy axis, therefore  $\mathbf{M} \perp \sigma$ , and magnetization was rotated over small angles by the pulsed oersted field  $H_p \sim 7$  Oe. Measurements were carried out at room temperature (295 K).

Element-specific XMCD hysteresis loops were taken as a function of transverse bias  $H_T$  to obtain a calibration for rotation angle  $\phi$  (Fig. 2). Photon energies were set to the  $L_3$  peaks for Fe (701 eV) and Ni (844 eV) to measure Fe and Ni XMCD signals, respectively (Fig. 2, left-hand side; nominal energies were close to reported peak energies of 707 eV and 853 eV, respectively). The XMCD signal is defined as the ratio of reflectivity difference to the reflectivity sum; reflectivity is taken as proportional to the photodiode drain current (reflected intensity), normalized to the reference grid electron yield current (incident intensity). The saturation values of XMCD signals are taken to be  $\phi_{\text{Ni}} = \phi_{\text{Fe}} = \pm 90^\circ$ . Well-defined hard-axis loop behavior is shown with an anisotropy field  $H_K$  of  $11.8 \pm 1.0$  Oe (Fig. 2, right-hand side); the Fe dichroism signal is roughly a factor of 2 larger than the Ni dichroism signal, consistent with previous work<sup>13</sup> and the smaller number of holes in Ni.

### III. RESULTS

The measurement of magnetization precession for Ni moments alone is presented in Fig. 3. XMCD signals were measured as a function of pump-probe delay and converted to time-dependent elemental Ni magnetization angles  $\phi_{\text{Ni}}(t)$  according to Fig. 2. Damped precessional oscillations are clearly seen, diminishing in amplitude ( $20^\circ$  to  $5^\circ$ ) and increasing in frequency (1.6 to 2.6 GHz) with increasing longitudinal bias  $0 < H_B < 100$  Oe.

Single-domain Landau-Lifshitz-Gilbert (LLG) simulations of Ni magnetization dynamics are plotted with the experimental data. Consistent parameters are used for the fits. These are  $M_s = 830$  kA/m, measured by SQUID from simultaneously deposited samples, and  $g_{\text{eff}} = 2.05$ . The  $g_{\text{eff}}^2 M_s$  products characterized by TR-XMCD agree within 6% to those found in Ref. 11, measured by PIMM. The anisotropy field  $H_K = 11.4 \pm 0.5$  Oe, determined according to the Kittel relationship  $\omega_p^2 = \gamma^2 \mu_0^2 M_s H_{\parallel}$  for in-plane magnetization precession and plotted in the right bottom panel of Fig. 3, agrees within experimental error with that measured statically by element-resolved hysteresis loops (Fig. 2, right-hand side). The pulse field  $H_p(t)$  was taken to be proportional to the

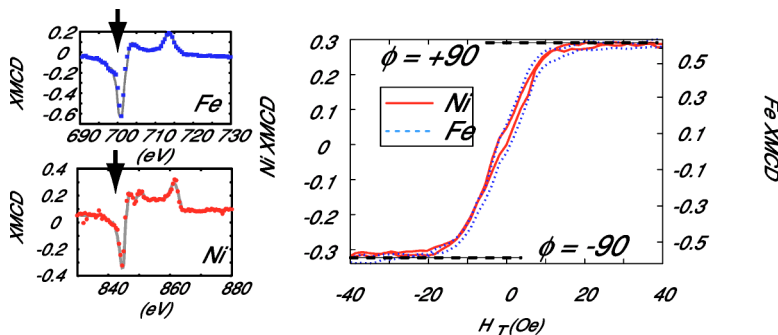


FIG. 2. (Color online) Left-hand side XMCD spectra over  $L_3$  and  $L_2$  edges for Ni and Fe. Photon energy was set to the  $L_3$  peak for Ni and Fe before measurement of element-specific hysteresis loops (right-hand side). The signal provides a calibration for the elemental magnetization angles  $\phi_{\text{Ni}}$  and  $\phi_{\text{Fe}}$ .

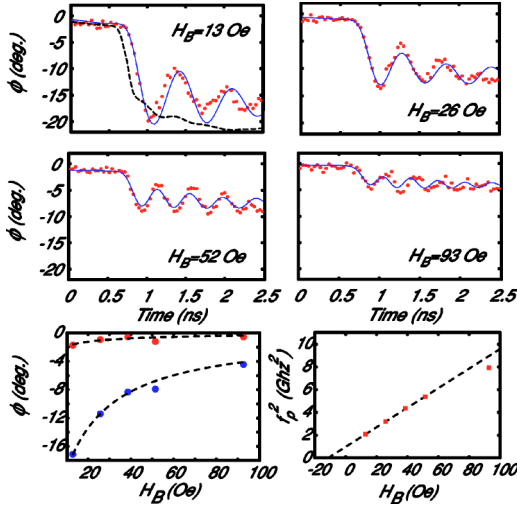


FIG. 3. Time dependence of Ni magnetization angle  $\phi_{Ni}(t)$  after falling magnetic field (points), with LLG simulation (lines). Top left;  $H_B=13$  Oe. Top right,  $H_B=26$  Oe. The wave form of the current pulse is indicated. Middle left,  $H_B=52$  Oe. Middle right,  $H_B=93$  Oe. Bottom left, equilibrium magnetization angles for high and low pulse levels; bottom right, Kittel plot of extracted precessional frequencies.

transmitted current wave form  $i_{pulse}(t)$  at the oscilloscope; scaling for the pulse was found by fitting the steady-state pre- and post-falling edge levels of magnetization angle  $\phi_{Ni}(0.5)$  and  $\phi_{Ni}(4.5)$  ns, respectively, yielding maximum pulse field level  $H_p=7.2$  Oe.

The Fe magnetization angles have been processed similarly. Differences between high and low saturation angles for Fe and Ni TR-XMCD scans ( $\Delta\phi_{Ni,Fe}$ ) are plotted in Fig. 4 as a function of longitudinal bias  $H_B$ . Agreement between experimental  $\Delta\phi_{Ni}(H_B)$ , experimental  $\Delta\phi_{Fe}(H_B)$ , and the single-domain model is satisfactory after application of an 11% increase in the XMCD-to- $\phi$  calibration factor found from the Fe hysteresis loop (Fig. 2). This level of adjustment is close to the level of drift measured in the saturation level of the Fe loop. High saturation levels of Fe are then offset to match those of Ni, by values varying from  $0^\circ$ – $2^\circ$ .

Element-specific precession is shown in Fig. 5. Ni and Fe moments are shown to precess together within instrumental

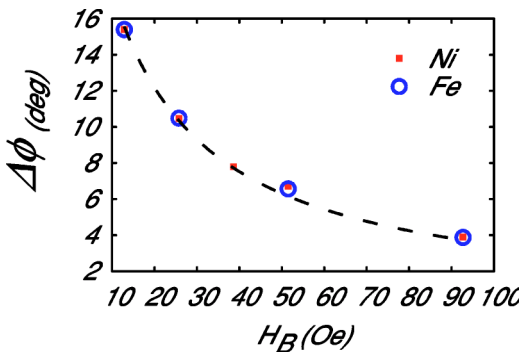


FIG. 4. (Color online) Differences between high and low saturation angles of the elemental Ni and Fe scans during TR-XMCD measurement,  $\Delta\phi = \phi(t=0.5 \text{ ns}) - \phi(t=4.5 \text{ ns})$ . Measured points for Ni and Fe are shown with the single-domain model fit.

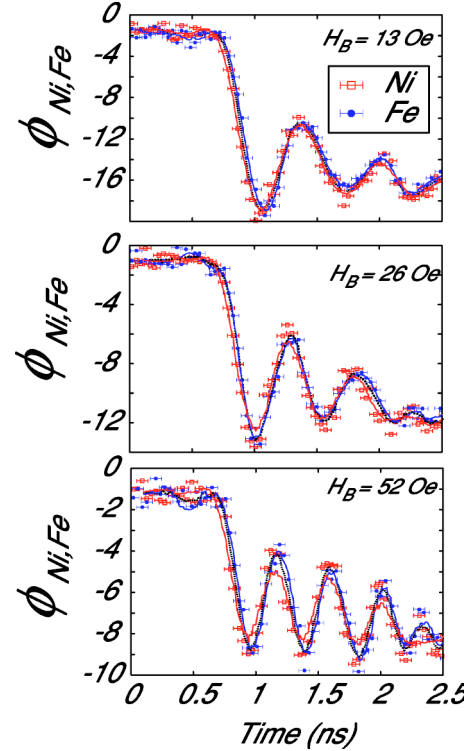


FIG. 5. (Color online) TR-XMCD measurement of Fe and Ni magnetization angle during free precession. Top,  $H_B=13$  Oe. Middle,  $H_B=26$  Oe. Bottom,  $H_B=52$  Oe. Solid lines are polynomial smoothing functions applied to the Fe and Ni data sets separately; dotted lines are polynomial smoothing functions applied to Fe and Ni data sets together. Timing errors of  $\pm 45$  ps are indicated.

resolution ( $\pm 45$  ps). As the longitudinal bias field  $H_B$  increases, the precessional frequency increases for both elements and there is no apparent development of a phase lag greater than experimental error.

#### IV. DISCUSSION

Ni and Fe magnetic moment precession is observed to be coupled in phase, within 90 ps, during FMR precession of  $Ni_{81}Fe_{19}$ . The measurement provides direct experimental confirmation that the net Fe and Ni elemental moments are collinear during precession at time scales exceeding 90 ps. It should be noted that this result could not have been easily determined without assumption from existing measurement techniques such as PIMM or time-resolved magneto-optical Kerr effect.

The result indicates that the exchange force exceeds the tendency of moments on Ni and Fe to precess or relax at different rates. The time resolution of the experiment is on the order of the spin-lattice relaxation time  $\tau_{sl}$  characterized for Gd,<sup>14</sup>  $100 \pm 80$  ps, which characterizes the direct spin-to-lattice relaxation channel; these values are unknown for transition metals but can be expected to be within an order of magnitude. A tendency for Fe and Ni moments to relax at different rates is plausible based on the orbital to spin moment ratios  $L/S$  of Ni and Fe characterized in  $Ni_{81}Fe_{19}$  by XMCD, 0.12 and 0.08, respectively.<sup>6</sup>

The prospect of partially coupled motion is more likely in systems where exchange coupling is weaker and/or magnetic moments are more localized. Transition-metal-rare-earth alloys, featuring lower Curie temperatures and more isolated  $f$  shells on the rare earths, would be attractive systems to study using the technique. Many rare-earth dopants in  $\text{Ni}_{81}\text{Fe}_{19}$  have been found to increase the FMR loss,<sup>11</sup> and TR-XMCD can test the possibility that some loss is carried by a phase lag between RE and TM moments.<sup>15</sup> Similarly, the trilayer structures used in spin electronics (e.g., NiFe/Cu/CoFe) offer the possibility of continuous adjustment of interlayer coupling through the spacer thickness.

Finally, we note the possibility of additional studies through more detailed spectroscopic information. Spin and orbital moment dynamics may be separated on individual elements through the use of sum rules. We take the point time resolution as that of the measurement; it should be noted that edge resolution, with long enough averaging and continuous monitoring for drift of the pulse amplitude  $H_p$ , could be improved. Better control over pulse delivery jitter will allow a point resolution limited only by  $\sigma_{ph}$  and longer averaging could allow edge resolution better than that of the lower bound of  $\tau_{st}$ .

## V. CONCLUSION

We have separated Ni and Fe moment motion in  $\text{Ni}_{81}\text{Fe}_{19}$  by TR-XMCD, demonstrating elemental resolution in ferromagnetic resonance up to 2.6 GHz. Coupled motion of elemental moments is found to a time resolution of  $\pm 45$  ps and an angular resolution better than  $2^\circ$ .

## ACKNOWLEDGMENTS

The authors thank Gary Nitzel (NSLS) for technical support. This work was partially supported by the Army Research Office, Grant No. ARO-43986-MS-YIP. Use of the Advanced Photon Source was supported by the U. S. Department of Energy, Office of Science, Office of Basic Energy Sciences, under Contract No. W-31-109-Eng-38. Research was carried out in part at the National Synchrotron Light Source, Brookhaven National Laboratory, which is supported by the U.S. Department of Energy, Division of Materials Sciences and Division of Chemical Sciences, under Contract No. DE-AC02-98CH10886.

---

\*URL: <http://magnet.ap.columbia.edu>

<sup>1</sup>I. Malajovich, J. Kikkawa, D. Awschalom, J. Berry, and N. Samarth, *Phys. Rev. Lett.* **84**, 1015 (2000).

<sup>2</sup>J. Marohn, P. Carson, J. Hwang, M. Miller, D. Shykind, and D. Weitekamp, *Phys. Rev. Lett.* **75**, 1364 (1995).

<sup>3</sup>M. van Schilfgaarde, I. Abrikosov, and B. Johansson, *Nature (London)* **400**, 46 (1999).

<sup>4</sup>K. Mikke, J. Jakowska, Z. Osetek, and A. Modrzejewski, *J. Phys. F: Met. Phys.* **7**, L211 (1977).

<sup>5</sup>T. Schulthess (private communication).

<sup>6</sup>E. Foy, S. Andrieu, M. Finazzi, R. Poinso, C. Teodorescu, F. Chevrier, and G. Krill, *Phys. Rev. B* **68**, 094414 (2003).

<sup>7</sup>M. Farle, *Rep. Prog. Phys.* **61**, 755 (1998).

<sup>8</sup>C. Chen, Y. Idzerda, H.-J. Lin, N. Smith, G. Meigs, E. Chaban, G. Ho, E. Pellegrin, and F. Sette, *Phys. Rev. Lett.* **75**, 152 (1995).

<sup>9</sup>M. Bonfirm, G. Ghiringhelli, F. Montaigne, S. Pizzini, N. Brookes, F. Petroff, J. Vogel, J. Camarero, and A. Fontaine, *Phys. Rev. Lett.* **86**, 3646 (2001).

<sup>10</sup>A. Kos, T. Silva, and P. Kabos, *Rev. Sci. Instrum.* **73**, 3563 (2002).

<sup>11</sup>S. Reidy, L. Cheng, and W. Bailey, *Appl. Phys. Lett.* **82**, 1254 (2003).

<sup>12</sup>A. Lumpkin (private communication).

<sup>13</sup>O. Eriksson, B. Johansson, R. Albers, A. Boring, and M. Brooks, *Phys. Rev. B* **42**, 2707 (1990).

<sup>14</sup>A. Vaterlaus, T. Beutler, and F. Meier, *Phys. Rev. Lett.* **67**, 3314 (1991).

<sup>15</sup>B. Clarke, K. Tweedale, and R. Teale, *Phys. Rev.* **139**, A1933 (1965).